A R C H I V E S O F M E T A L L U R G Y A N D M A T E R I A L S
Volume 60 2015 Issue 2
DOI: 10.1515/amm-2015-0180

T. KVAČKAJ*,♯, A. KOVÁČOVÁ*, J. BIDULSKÁ*, R. BIDULSKÝ*, R. KOČIŠKO*

NEW APPROACH IN THE PROPERTIES EVALUATION OF ULTRAFINE-GRAINED OFHC COPPER

NOWE PODEJŚCIE DO OCENY WŁAŚCIWOŚCI ULTRA DROBNOZIARNISTEJ MIEDZI OFHC

In this study, static, dynamic and tribological properties of ultrafine-grained (UFG) oxygen-free high thermal conductivity (OFHC) copper were investigated in detail. In order to evaluate the mechanical behaviour at different strain rates, OFHC copper was tested using two devices resulting in static and dynamic regimes. Moreover, the copper was subjected to two different processing methods, which made possible to study the influence of structure. The study of strain rate and microstructure was focused on progress in the mechanical properties after tensile tests. It was found that the strain rate is an important parameter affecting mechanical properties of copper. The ultimate tensile strength increased with the strain rate increasing and this effect was more visible at high strain rates ($\dot{\varepsilon} \sim 10^2$ s^{-1}). However, the reduction of area had a different progress depending on microstructural features of materials (coarse-grained vs. ultrafine-grained structure) and introduced strain rate conditions during plastic deformation (static vs. dynamic regime). The wear behaviour of copper was investigated through pin-on-disk tests. The wear tracks examination showed that the delamination and the mild oxidational wears are the main wear mechanisms.

Keywords: OFHC copper, UFG, ECAP, strain rate, fractography, wear resistance

W pracy zbadano szczegółowo statyczne, dynamiczne i tribologiczne właściwości ultra drobnoziarnistej (UFG) beztlenowej miedzi o wysokiej przewodności cieplnej (OFHC). W celu oceny właściwości mechanicznych przy różnych szybkościach odkształcenia, miedź OFHC badano za pomocą dwóch urządzeń w warunkach statycznych i dynamicznych. Ponadto miedź poddano dwóm różnym sposobom przetwarzania, co umożliwiło badanie wpływu struktury. Badanie szybkości odkształcenia i mikrostruktury koncentrowało się na zmianie właściwości mechanicznych po próbie rozciągania. Stwierdzono, że szybkość odkształcania jest ważnym parametrem wpływającym na właściwości mechaniczne miedzi. Wytrzymałość na rozciąganie wzrosła ze wzrostem szybkości odkształcenia i ten efekt był bardziej widocznyprzy dużej szybkości odkształcania ($\dot{\varepsilon} \sim 10^2$ s^{-1}). Jednak zmniejszenie obrazu przebiegało inaczej w zależności od cech mikrostruktury materiałów (struktura gruboziarnista a struktura ultra drobnoziarnista) i zadanych warunków szybkości odkształcenia podczas odkształcenia plastycznego (warunki statyczne a warunki dynamiczne). Zużycie miedzi badano za pomocą testów zarysowania. Badanie ścieżek zużycia wykazało, że delaminacja i umiarkowane utlenienie to główne mechanizmy zużycia.

1. Introduction

It is well known that the mechanism of plastic deformation in ultrafine-grained (UFG) and nanostructured materials proceeds differently compared to the classical coarse-grained (CG) materials. Generally, plastic deformation in polycrystalline materials is carried out by mechanism as dislocations movement, vacancies diffusion and grain boundaries sliding. Hence, ultimate plastic deformation includes all of these processes and strongly depends on deformation conditions as strain, temperature, stress, creep conditions, strain rate etc. Considering materials with mean grain size below 1 μm (UFG, nanostructured), the fraction of atoms within and near grain boundaries can increase exponentially. Consequently, the plastic deformation processes which are managed by grain boundary (grain boundary diffusion, grain boundary sliding) could be activated [1,2]. At the present time, to study unique microstructural and substructural features forming in materials during plastic deformation methods based on electron microscopy (TEM, SEM, HRTEM, EBSD) have been successfully applied [3-5].

One of the main advantages of UFG and nanostructured materials is suitable combination between strength and plasticity [6]. The high strength at room temperature is connected with ductility loosing in classical coarse-grained materials. Consequently, its practical application is limited. It is supposed that some nanocrystalline metallic alloys and ceramic materials show superplasticity at lower temperatures and for higher strain rates [7,8] in comparison to its coarse-grained counterparts. Some experimental results also imply opportunity of nanostructured materials to achieve high diffusion rate [9-11].

* DEPARTMENT OF METAL FORMING, FACULTY OF METALLURGY, TECHNICAL UNIVERSITY OF KOŠICE, SLOVAKIA
♯ Corresponding author: tibor.kvackaj@tuke.sk

1.1. Severe plastic deformation (SPD)

Nowadays, several available production methods of nanocrystalline and ultrafine-grained materials have been used. These methods can be divided into following groups:

a) mechanical alloying (including cryomilling) and following compaction [12,13],
b) severe plastic deformation [14,15],
c) gas-phase condensation of particles and consolidation [16,17],
d) electrodeposition [18,19].

While the first two methods usually lead to ultrafine-grained structure formation, other two methods are also used for materials production with mean grain size in the tens of nanometer.

The material processing through severe plastic deformation methods is defined as a metal forming process in which a great strain is introduced to samples. Nevertheless, sample parameters after processing remain almost the same in many cases. As a result, strong grain refinement is obtained [20].

The following methods belong to the group of severe plastic deformation [21-25]:

- pressing: high-pressure torsion (HPT), multiaxial forging (MF),
- extrusion: equal-channel angular pressing (ECAP), equal-channel angular rolling (ECAR), cyclic-extrusion-compression (CEC), twist extrusion (TE), KOBO,
- rolling: accumulative roll-bonding (ARB), rolling + axial rolls shifting (RRS), linear flow splitting (LFS),
- corrugation: repetitive corrugation and straightening (RCS),
- friction: friction stir processing (FSP).

All of them are able to introduce great amount of plastic deformation into the sample and consequently to obtain significant grain refinement. Some of them as ECAP, HPT and ARB are well-known methods for processing the materials with ultrafine-grained (UFG) structure. Final microstructure may contain grain size in the range d ~10-500 nm depending on crystal lattice and applied SPD method [20].

1.2. Equal Channel Angular Pressing (ECAP)

ECAP is a promising method due to following reasons:

1. it is simple and can be used in various alloys processing,

2. ECAP is suitable for producing the materials with various crystal lattice and various structure conditions (precipitation hardened alloys, intermetallic compound, composite with metallic matrix).

3. suitable structure homogeneity is achieved after several sample passes.

Owing to these attractive features, a lot of experimental studies focused on the development of ECAP method have been performed in recent years [24-27].

ECAP equipment is schematically illustrated in Fig. 1 [28]. The ECAP die contains two intersecting channels. The angle between channels is called as a main angle Φ. The place where channels are intersected is also characterised by additional angle ψ which presents outer radius of the die. Within ECAP process, the sample in cylindrical or square cross section is being pressed through the die by using piston (Fig. 1).

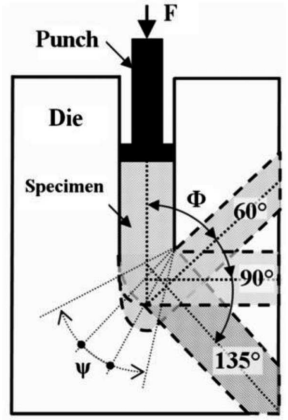

Fig. 1. Schematic illustration of ECAP equipment [18]

As it is seen in the Fig. 1, one of the main features of ECAP is an emerging almost pure shear during processing. Besides, although great deformation is introduced to the sample, no changes in the sample parameters are observed. Unchanged cross-section of the sample presents difference between traditional (rolling, drawing, pressing) and new SPD methods of metal forming [17]. During ECAP processing, samples are pressed through a die several times in order to obtain great deformation and structural homogeneity. Repeated passes provide opportunity to active the different shear systems through simple sample rotation before each pass [29]. The number of ECAP passes is also one of the most important parameter affecting material properties. It is well known that the most significant microstructure refinement takes place during the first ECAP pass [17]. Subsequent ECAP passes provide specific microstructural features formation resulting in atypical mechanical properties behaviour [30].

1.3. Mechanical properties in materials processed by SPD methods

It is well-known that strength and plasticity are key material mechanical properties. In materials with coarse-grained (CG) structure they have an inverse character. It is highly likely, that this is not valid in UFG materials just due to different plastic deformation mechanism developed during the processing [17]. Moreover, some experimental studies provide occurrence of superplasticity at low temperature as well as at high strain rate in UFG metals [31,32]. These issues are important for the prospective development of high strength and wear resistance as well. On the other hand, advanced superplastic alloys and metals have high fatigue properties. Therefore, there is growing interest in research to combine good mechanical and functional properties in UFG materials subjected to ECAP.

The grain refinement to nanometer scale in various metals and alloys leads to high strength and still suitable plasticity after tensile tests. The authors [33] investigated Al-3004 alloy processed by ECAP and rolling methods at room temperature. The experimental results are schematically shown in Fig. 2 [34]. The strength increased gradually with the increasing strain in both cases (rolling and ECAP). On the other hand, it is also seen that ultimate ductility showed a different progress in dependence on applied technology. After 1 ECAP pass, ductility decreased from ~32% to ~14%. The subsequent ECAP passes have not such significant influence on the

ductility, therefore greater deformation can be applied. The rolling method provides great initial reduction in the ductility and this tendency is also visible after following processing. As a result, an ECAP method offers more advantageous combination of mechanical properties compared to conventional rolling at room temperature.

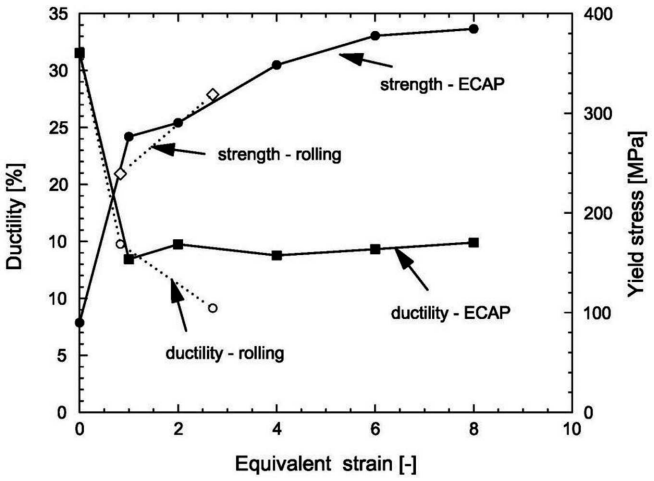

Fig. 2. Comparison between yield stress and ductility for the Al-3004 alloy processed by cold-rolling or ECAP [34]

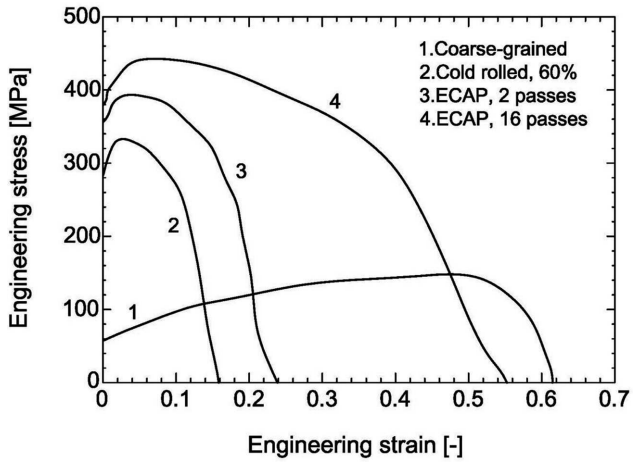

Fig. 3. Tensile engineering stress-strain curves for Cu tested at 22°C with a strain rate of $10^{-3}s^{-1}$ [35]

In the next experimental study, high purity Cu (99.996%) was also processed by an ECAP and a rolling method [35]. The strength and plastic properties were determined by an uniaxial tensile test and the experimental results are schematically illustrated in Fig. 3 [35]. The tensile tests were carried out at room temperature. It is clear that initial coarse-grained Cu showed low yield stress but great plastic properties. Using rolling at room temperature (60% thickness reduction), strength increased significantly but plasticity was reduced considerably (curve 2), after 2 ECAP passes there was a similar progress (curve 3). Such behaviour is in accordance with classical metal strain hardening developed during plastic deformation. However, curve 4 illustrates Cu behaviour processed by 16 ECAP passes where additional strengthening along with growing ductility is shown.

1.4. Strain rate effect

The strain rate is a significant parameter affecting mechanical properties of metallic materials, especially at higher strain rates ($\dot{\varepsilon}$ >300 s^{-1}) [36]. Therefore, the influence of high strain rate on mechanical properties requires further research.

In general, classical tensile equipments provide sample loading at strain rate up to 1 s^{-1}. In order to obtain the strain rate up to 100 s^{-1}, modern hydraulic systems have been applied [37]. However, there are a few experimental studies focused on the strain rate influence performed in the range of 100-1000 s^{-1} on materials with UFG structure. Most of the experimental studies have been nowadays focused on determination of the material strain rate sensitivity [38, 39]. For these purposes equipments as a Kolsky and Hopkinson bar have been successfully applied to achieve the strain rate above 1000 s^{-1} [38]. A rotating flywheel has been used as a device for studying the strain rate in the range of 100-1000 s^{-1}. Flywheels provide great kinetic energy that is much greater than energy required for the sample deformation resulting at constant velocity of the machine [38].

The experiment focused on the study of strain rate on copper properties through different experimental devices was performed in Ref. [39]. The progress in flow stress on strain rate is schematically shown in Fig. 4 [39]. According to this study, the material flow stress increased with the strain rate increasing what implies the significant material sensitivity to the strain rate.

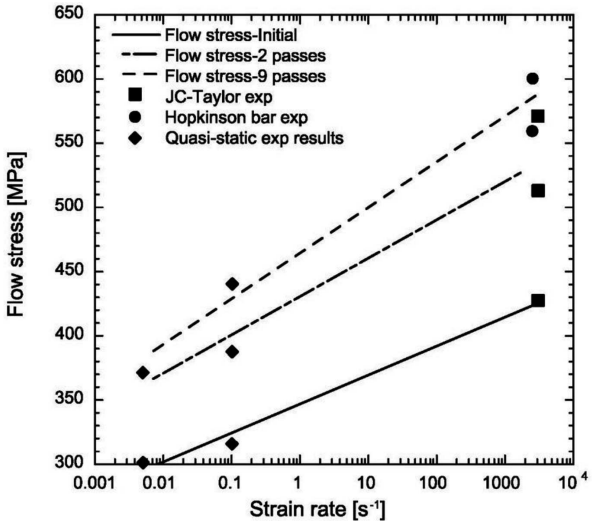

Fig. 4. Strain-rate dependence of Cu flow stress [39]

Main objective of this paper was to study the changes in mechanical properties of ultrafine-grained OFHC copper (processed by ECAP) in the wide range of strain rates. Since the copper was also subjected to drawing, there was able to consider the influence of initial microstructure (ultrafine-grained vs. coarse-grained). Moreover, the experiment was extended to the study of wear characteristics through pin-on-disc wear tests.

2. Experimental material and methods

Initial material for this study was OFHC (oxygen free high conductivity) Cu (99.99+%). Such copper is produced by direct conversion of selected refined cathodes and castings under carefully controlled conditions due to contamination of the pure oxygen-free metal during processing. Cu sample were pressed through the ECAP die ($\varphi = 90°$) with 5 passes and rotated by route C. In order to study the influence of microstructure, two plastic deformation methods have been used and performed at room temperature. Drawing was applied as a classical method for producing the samples with coarse-grained (CG) and ECAP as a new, progressive method for producing the samples with ultrafine-grained (UFG) structures.

The study of strain rate was carried out in the wide strain rate range and hence two testing regimes had to be defined: static ($\dot{\varepsilon} \sim 10^{-3}$ - 10^{-1} s^{-1}) and dynamic ($\dot{\varepsilon} \sim 10^{2}$ s^{-1}). The tensile tests were performed at room temperature. The classical tensile testing machine Labtest 5.20 with strain gauge was used in order to static conditions investigation. For the purpose of dynamic conditions investigation a rotating flywheel machine with a piezoelectric detector was applied. The geometrical parameters of samples used for static and dynamic tensile tests are illustrated in Fig. 5.

The achieved experimental results were processed by mathematical analysis using software products as a MS Excel, Matlab and program „R".

For tribological properties, there was done 4 and 6 ECAP passes through the route C. Specimens were obtained using an orbital press (OF), applying a pressure of 200 MPa at logarithmic strain of 1.95.

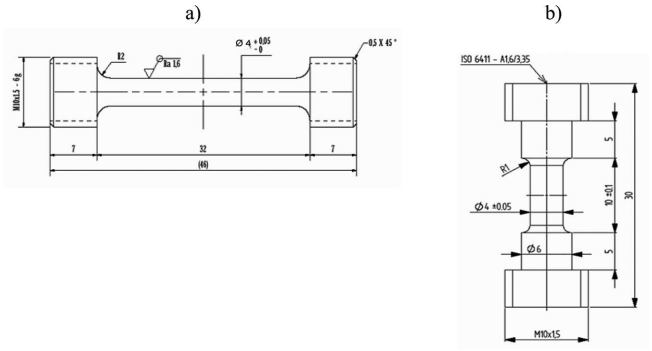

Fig. 5. The geometrical parameters of samples [mm] for a) static b) dynamic conditions

Pin-on-disc wear tests were carried out, the disc was made from the investigated material. As a counter face, a WC-Co pin was used, having a rounded shape on top with diameter 3 mm. The counter-pin was changed after the end of each test, in order to preserve the roundness of its top. All wear tests were performed in air and without any lubricant. The applied load was 15 N. The rotation speed of the disc was 300 rpm. The tested surface was polished with abrasive papers in order to obtain a medium surface roughness equal to (or less than) 0.8 μm, as specified in the ASTM G99-95a. Each test was interrupted after 300, 600, 900, 1200, 2000, 3000, 4000 and 5000 meters sliding distance and discs were weighed to determine the evolution of wear during each test. The total sliding distance was monitored on an auto-recorder. The surface topography was measurement by Hommel Tester T1000 tangent profilometer and average values were obtained from 5 measurements.

All microstructural observations were carried out using SEM JEOL 7000F.

3. Results and discussion

Dependences of mechanical properties on the strain rate for the samples processed by drawing and ECAP in static conditions are shown in Figs. 6 and 7. According to graphs, the values of yield stress imply no significant difference between drawing and ECAP methods. After ECAP, even from $\dot{\varepsilon} \sim 0.1$ s^{-1}, a slight increase in the yield stress was achieved. On the other hand, the progress of ultimate tensile strength revealed influence of the applied methods on properties but still not so much significant. Considering reduction of area, it seems that applied methods have a huge impact on the progress because that was opposite to the strain rate increase (Figs. 6, 7).

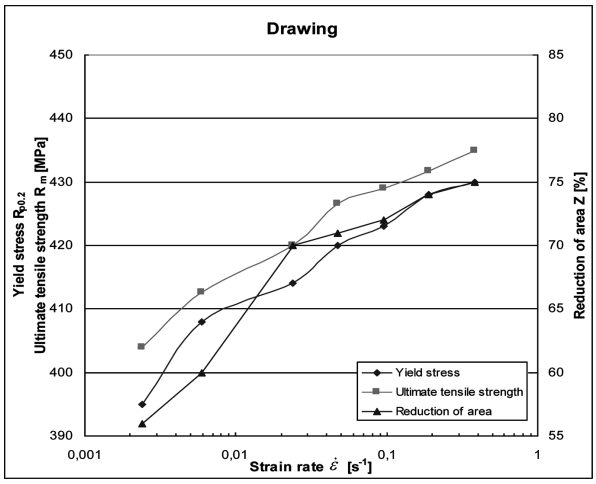

Fig. 6. The mechanical properties dependence on strain rate for drawing samples

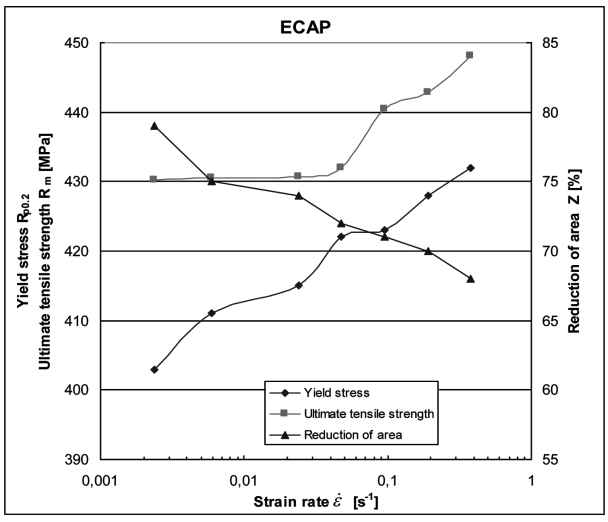

Fig. 7. The mechanical properties dependence on strain rate for ECAP samples

Fig. 8 is an example showing the data outgoing from dynamic tensile tests. On the screen of a detector, there was

recognized the wave coming from great dynamics of the whole testing process. The wave was visible from the point indicated by a dashed arrow in Fig. 8. The test was finished when a load dropped to the zero point (solid arrow in Fig. 8). The presence of waves was noticed throughout to whole dynamic regime for both states (drawing, ECAP).

The $R_{p0.2}$ was not established in the dynamic regime due to its nearly incidental value with R_m.

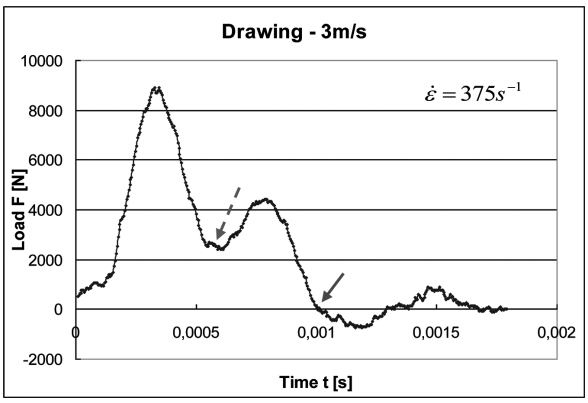

Fig. 8. The dependence of load on time for a drawing state (3 m/s)

Fig. 9 shows the ultimate tensile strength and reduction of area progress in dependence on strain rate for both states (drawing, ECAP). It is clear that ultimate tensile strength increases, however reduction of area decreases with the strain rate increasing. The evolution in mechanical properties is similar for both states that implies no significant microstructural influence on the mechanical properties progress in a dynamic regime.

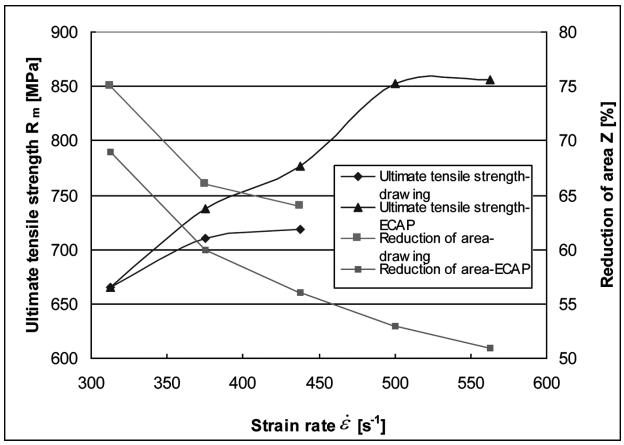

Fig. 9. The progress of mechanical properties in dependence on the strain rate in a dynamic regime

The dependence between mechanical properties and strain rate was linearized (Fig. 10). It was found that the strain rate increase can result in the changes of mechanical properties as follows:

- drawing state: R_m – increase about 4 MPa, Z – decrease about 0.8 % per 10 s^{-1}.
- ECAP state: R_m – increase about 8 MPa, Z – decrease about 1.0 % per 10 s^{-1}.

Hence, strength of the material processed by ECAP increases two times with the increasing strain rate in comparison to drawing however, the loss in plastic properties is almost the same for both methods.

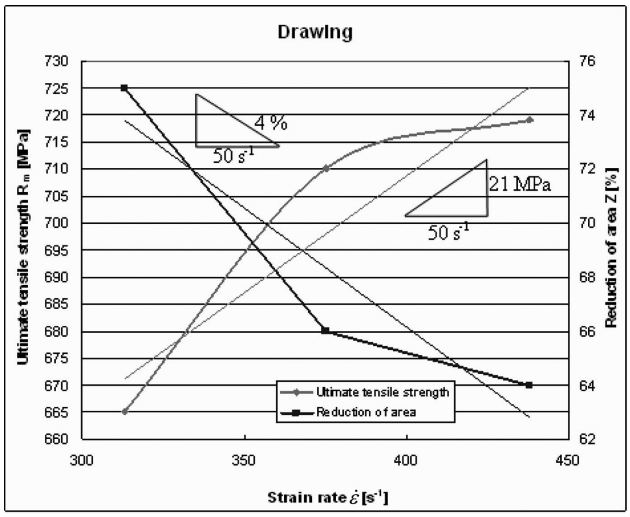

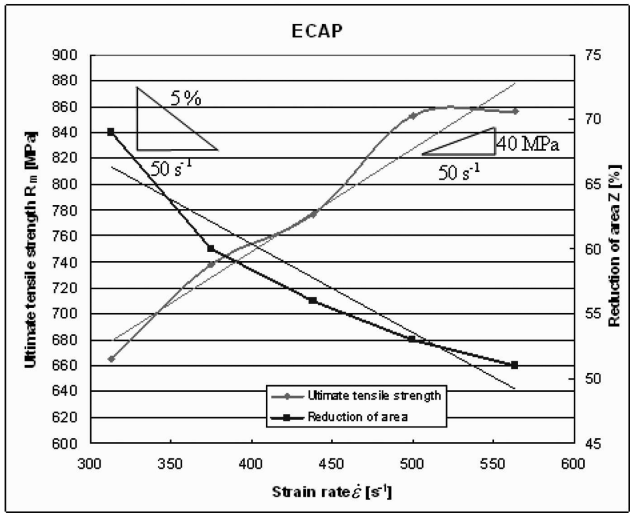

Fig. 10. Linearized progress of mechanical properties in a dynamic regime for a) drawing b) ECAP states

Experimental results which are described above were also processed by the mathematical method of nonlinear regression (method of the least squares). The relation between ultimate tensile strength (R_m) and strain rate ($\dot{\varepsilon}$) is described by Eqs. (1) and (2) for drawing and ECAP states, respectively.

$$R_{m_{Drawing}} = 408 + 32.53 \times 1.45^{\ln \dot{\varepsilon}} \quad (1)$$

$$R_{m_{ECAP}} = 436 + 0.78 \times 2.72^{\ln \dot{\varepsilon}} \quad (2)$$

The calculated and measured data were plotted to Figs. 11 and 12. From graphical dependences, a close agreement between data was found which is also confirmed by the correlation index (I). The correlation index is 0.998 and 0.997 for Eq. 1 and Eq. 2, respectively.

Since tensile tests were carried out in dynamic and static regimes, there was able to investigate the influence of strain rate on OFHC Cu mechanical properties in a wide range from 10^{-3} - 10^{-1} s^{-1} to 10^{2} s^{-1}. At the same time, tested samples were in CG state after drawing and UFG state after ECAP processing. Consequently, there was able to study the influence of microstructural features.

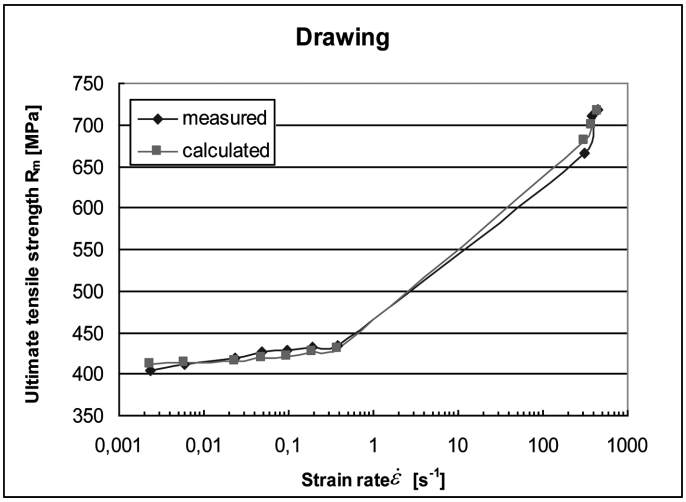

Fig. 11. Measured and calculated data of ultimate tensile stress for a drawing state

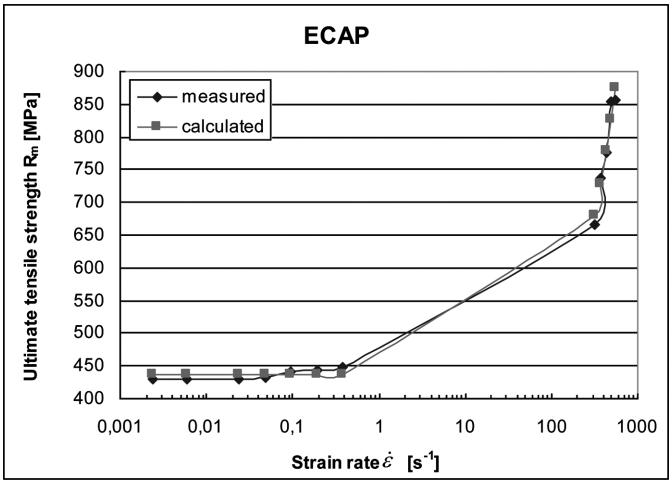

Fig. 12. Measured and calculated data of ultimate tensile stress for a ECAP state

Fig. 13 provides the overview in the development of mechanical properties in static and dynamic regimes for both structural states (CG and UFG). The static regime ($\dot{\varepsilon} \sim 10^{-3}$ - $10^{-1}\,s^{-1}$) can be characterised by gentle increase of the ultimate tensile strength with the increasing strain rate and an inverse progress in the reduction of area for both processing states. Besides, it is well-known that UFG materials provide higher strength and still advantageous plastic properties in comparison to CG materials. This is the main advantage of materials processed by SPD methods. It is expected that the dislocations movement in the samples with CG structure is more developed than in the UFG samples. It is assumed that UFG structure includes a large volume of grain boundaries which impede dislocations movement. As dislocations are plastic flow carriers, consequently plastic properties within ultrafine grains could be less developed.

The dynamic regime ($\dot{\varepsilon} > 300\ s^{-1}$) is characterised by rapid increase in the strength and by decrease in the plasticity with the strain rate increasing. The influence of microstructure is not so significant in the dynamic regime as was seen in the static one. Moreover, curves showing strength and plasticity in Fig. 13 have a stormy progress which clearly shows great material strain rate sensitivity in a dynamic regime.

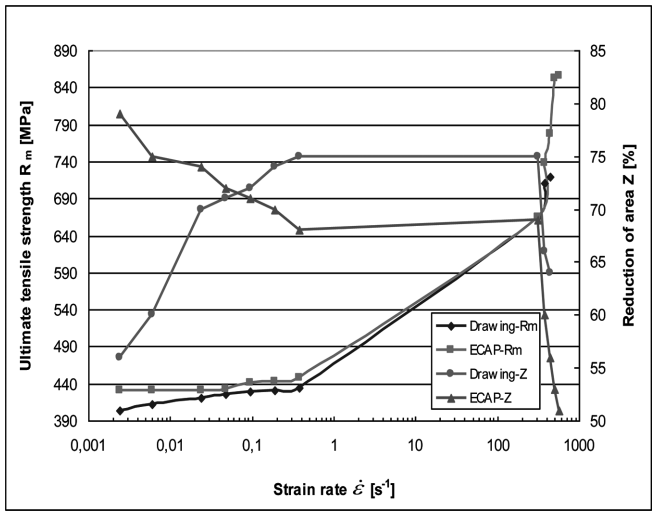

Fig. 13. The comparison in material properties in static and dynamic regimes

Fractography analysis

After static and dynamic tensile tests, fractured surfaces of samples were investigated. Typical micrographs are shown in Figs. 14 and 15. Based on the observation of fractured surfaces, a ductile fracture mode with typical dimple morphology in both strain rate regimes independent of applied experimental methods (drawing, ECAP) was found.

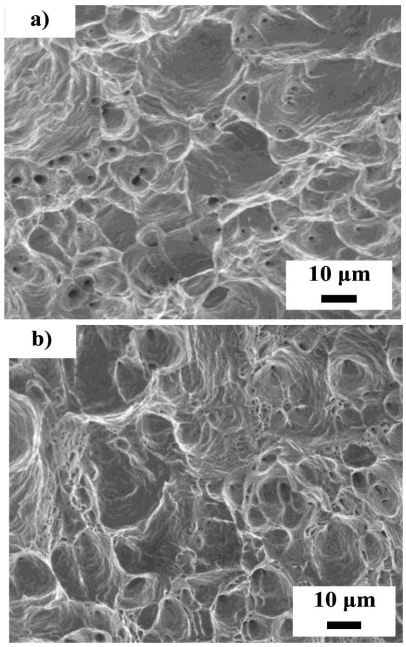

Fig. 14. SEM images of a) drawn b) ECAP samples after static tensile tests ($\dot{\varepsilon} \sim 10^{-3}\ s^{-1}$)

In order to investigate the strain rate effect, the fractured surfaces of ECAP samples after each imposed circumferential flywheel speed were subjected to fractography analysis. Again the ductile fractured mode with typical dimple morphology was found for all applied circumferential flywheel speed in a dynamic regime (Fig. 16).

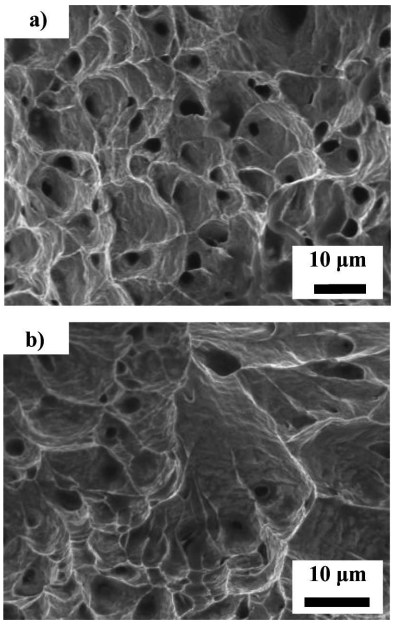

Fig. 15. SEM images of a) drawn b) ECAP samples after dynamic tensile tests ($\dot{\varepsilon}$ ~10^2 s^{-1})

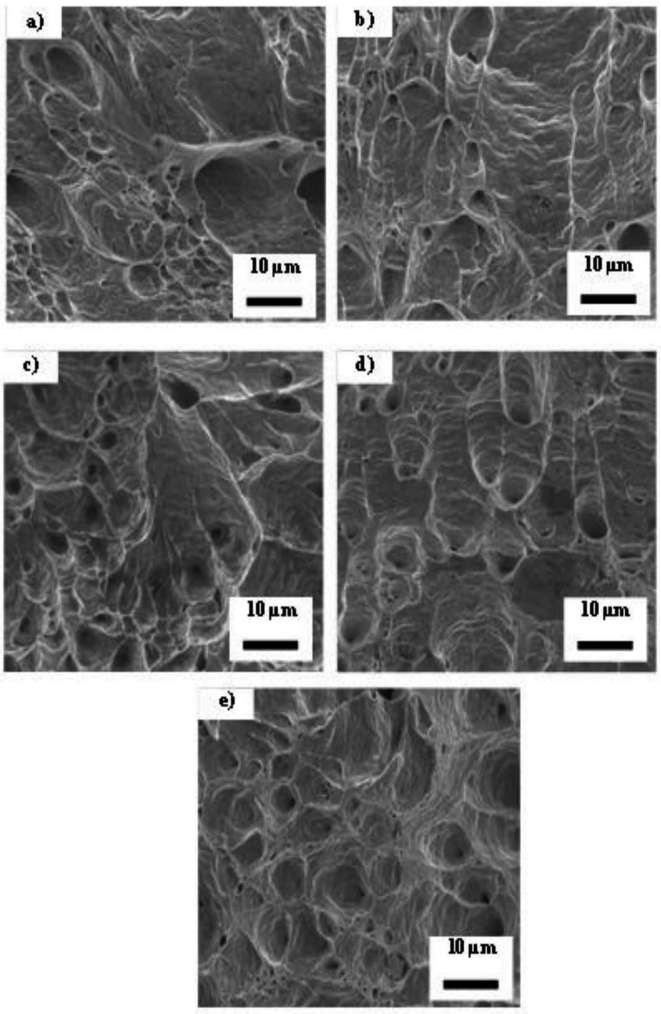

Fig. 16. Ductile fracture morphology of ECAP samples at circumferential flywheel speed: a) 2.0 m/s b) 2.5 m/s c) 3.0 m/s d) 3.5 m/s e) 4.0 m/s

4. The reduction of area and mean dimple size after dynamic tensile tests

The fractured surfaces of the ECAP samples after dynamic tensile tests were investigated in detail. The decrease in a mean dimple size with the increasing strain rate from 2.3 μm to 1.2 μm ($\dot{\varepsilon}$ ~200 - 400 s^{-1}) was found. The mean dimple size (d_{dimple}) was determined from a statistical file including 400 measurements. The obtained data in dependence on strain rate are given in Table 1.

TABLE 1

The obtained mean d_{dimple} and Z data

v [m/s]	$\dot{\varepsilon}$ [s^{-1}]	d_{dimple} [μm]	Z [%]
2.0	181	2.3	68.0
2.5	227	1.9	64.0
3.0	273	1.4	58.6
4.0	364	1.2	56.4

The obtained data are also schematically presented in Fig. 17. It was found that mean dimple size as well as reduction of area decrease with the increasing strain rate.

Experimental results which are described above were processed by the mathematical method of linear regression (method of the least squares). The relation between reduction of area (Z) and mean dimple size (d_{dimple}) is described by Eq. 3. The calculated and measured data were plotted in Fig. 18 and high agreement between the data with a correlation index (I) of 0.9998 was found.

$$Z = 43.25652 + 10.74244 \times d_{dimple} \tag{3}$$

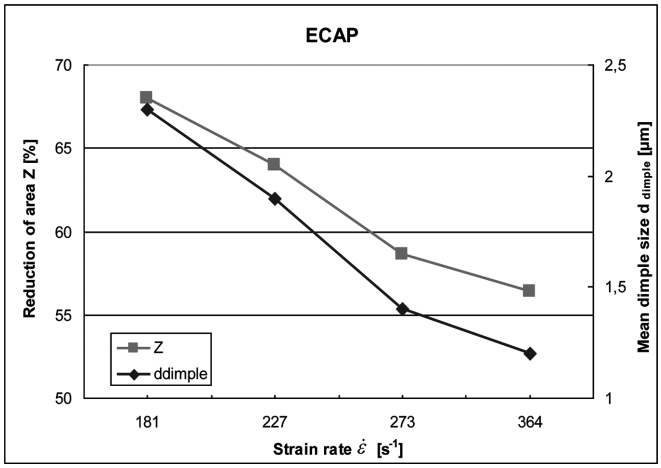

Fig. 17. The dependence in reduction of area and mean dimple size on strain rate

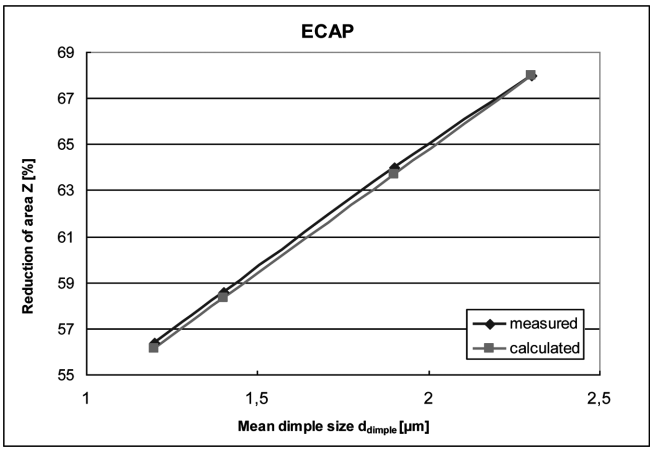

Fig. 18. Measured and calculated data of reduction of area and mean dimple size

5. Study of tribological properties

The friction coefficients versus dry sliding time curves are shown in Fig. 19. They can be divided into four stages. The initial value of the friction coefficient of Stage I, which is below 0.1 value of f_0, is dependent on the load, F_N, and on the shear resistance of surface contaminants. The higher value of f_0 was achieved in orbital forging system. The incremental deformation bulk forming process, represented by the orbital forming, led to smaller stresses with a reduction of shear deformation, which is present during ECAP process. The surface layer removal and an increase in adhesion due to the increase in clean interfacial areas, as well as increased asperity interactions and wear particle entrapment lead to a gradual increase in the friction coefficient.

Stage II represents the maximum values, producing the peak value of the friction coefficient. These results show the positive influence of the incremental deformation bulk forming process on reduction of the interfacial adhesion and asperity deformation.

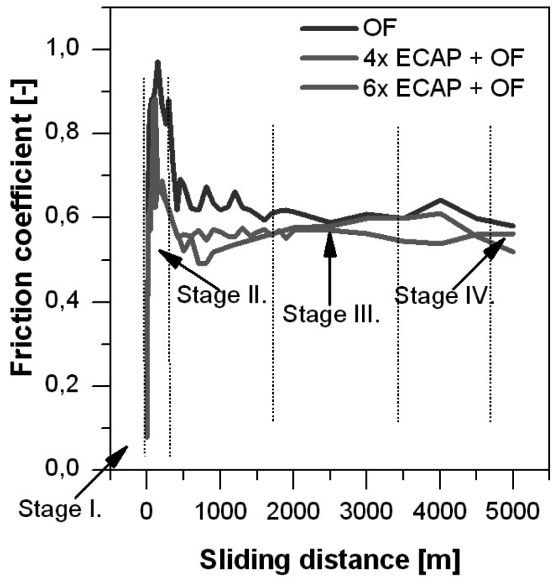

Fig. 19. Four stages of the friction coefficient

In Stage III, a decrease in the friction coefficient may occur, due to the possible formation of protective tribochemical surface layers and a decrease in plowing and asperity deformation processes in accordance with Blau [40]. In this stage constant friction coefficients were recorded. Therefore, the steady-state values of friction coefficient, $f_{steady-state}$ were determined corresponding to the steady-state interfacial tribological conditions.

In Stage IV the value of the friction coefficient is a bit smaller than that one of the steady-state. This may be attributed to the fact that initially the surface is rough, though with uneven asperities and contact temperatures (the surface temperatures) as well as the metal-to-metal contact causes different friction coefficient values at the end of the test, f_{final}.

TABLE 2

The results of surface topography

	Orbital forged	4 ECAP + orbital forged	6 ECAP + orbital forged
$f_{steady-state}[-]$	0.61	0.56	0.57
Rz [μm]	1.1	3.17	2.53
Ra [μm]	0.18	0.41	0.3
HV	248	317	593

From Table 2 results that the surface roughness values of both parameters Ra and Rz, should affect the value of friction coefficient along with hardness. Hanlon et al. [41] reported that strength/hardness rather than the grain size appeared to dominate the steady state friction coefficient and damage accumulation, with substantial increases in material strength. On the other hand, it is generally known [32-45] that a higher hardness does not always lead to a better wear resistance and hardness alone should not necessarily be considered the most critical factor in assessing the wear resistance of material. Several authors [46-48] present suggestions for correlation of wear behaviour with the surface topography. The fact that surface wear is influenced by sub-surface deformation [49-54] was also effectively used to show the occurrence of delamination and fracture of material resulting in its removal.

Experimental data about the role of subsurface evaluation in terms of workability is still limited, especially in a newly progressive processing – ECAP, orbital forming [55-57], where workability is one of the most important artefact in UFG materials, according to Kvačkaj [58]. The results of wear rate vs sliding distance are presented in Fig. 20.

It may be seen that the wear rate is significantly dependent on the processing condition. Wear rate decreases continuously in the running-in period and obtains the steady state, mainly in systems with SPD. The probability of the occurrence of elementary wear events may decrease if through changes in surface topography, the interaction rate of surface asperity collisions decreases. Figs 21-23 show that wear decrease significantly in systems with SPD compared to specimen without using SPD, because the fresh fractured surfaces can be easily oxidized in dry sliding and the oxidized debris on the worn surface can also be subjected to a complicated process of mixing, compacting and smearing under the repeated action of severe plastic deformation from the loading. The surface oxide layer can be better pressed into the base metal and precisely attached

to it. The mixed surface layer on the worn surface consists of compacted or accumulated debris and surface oxide layers. These surface asperities prevent the contact of metal to metal during the sliding.

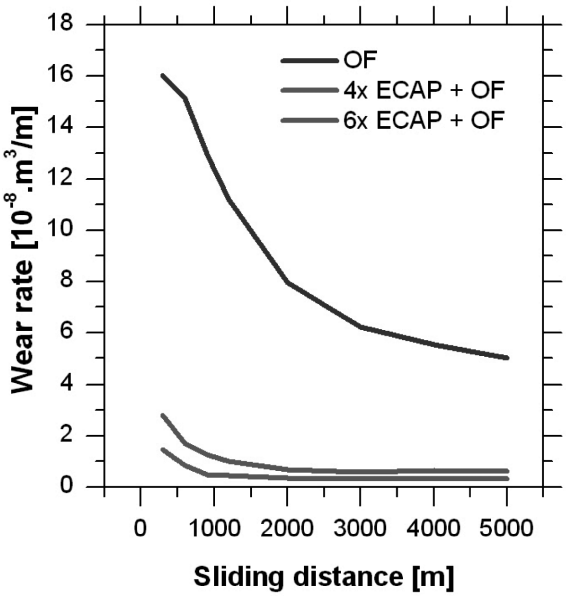

Fig. 20. The wear rate of studied materials

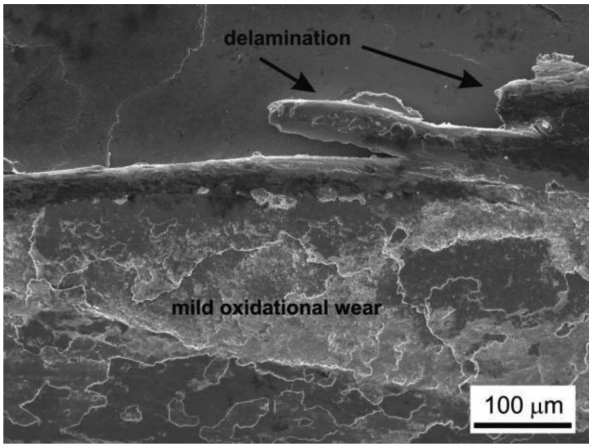

Fig. 21. SEM micrograph showing delamination and mild oxidational wear behaviour in system orbital forged

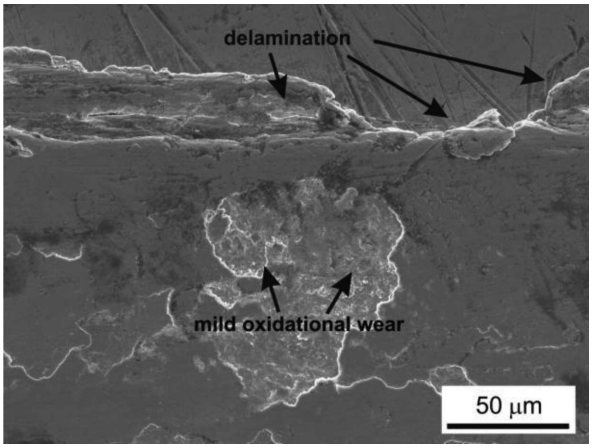

Fig. 22. SEM micrograph showing delamination and mild oxidational wear behaviour, 4 ECAP and OF

It can also be seen from Figs. 21-23 that also mild oxidational wear are present in all the investigated systems. The arrows indicate that the delamination and the mild oxidational wears were recorded to be the main wear mechanisms.

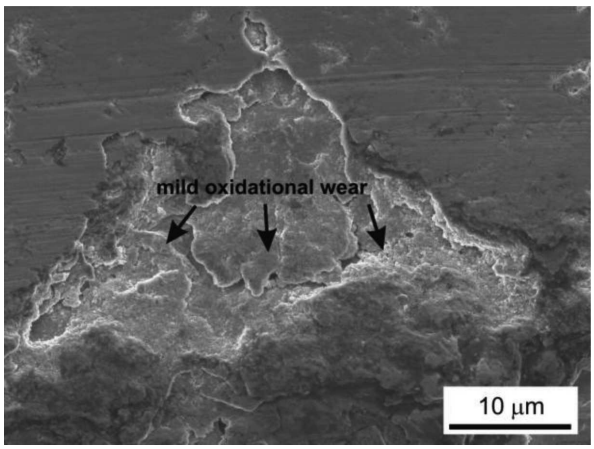

Fig. 23. SEM micrograph showing delamination and mild oxidational wear behaviour, 6 ECAP and OF

6. Conclusions

According to this study, following conclusions can be made:

- mechanical properties of OFHC Cu depend on strain rate, the dependence is stronger at a dynamic ($\dot{\varepsilon} \sim 10^2$ s^{-1}) than in a static ($\dot{\varepsilon} \sim$ from 10^{-3} to 10^{-1} s^{-1}) regime.
- strength properties are growing up with the strain rate increasing in both regimes.
- the progress in plasticity is unclear. In the static regime, the reduction of area has an inverse trend resulting from different microstructural characteristics (CG vs. UFG). Nevertheless, this tendency disappears in a dynamic regime where reduction of area was decreased with the increasing strain rate in both cases.
- linearization of the dependence between mechanical properties and strain rate shows that the strength in the samples processed by ECAP (UFG structure) increased two times with the increasing strain rate compared to drawing (CG structure) but the loss in plasticity was approximately the same.
- fracture investigation reveals no significant influence strain rate and microstructure influence on failure mechanism.
- the friction-time curve during dry sliding can be divided into four stages of friction coefficient changes.
- wear rate (represent the wear properties) decreases continuously in the running-in period and obtains the steady state.
- orbital forging and ECAP suppress the interfacial adhesion and asperity deformation.
- the delamination and the mild oxidational wears are the main wear mechanisms.

Acknowledgements

This work was financially supported by the VEGA 1/0325/14 project.

REFERENCES

[1] K.S. Kumar, H. Swygehnoven, S. Suresh, Acta Materialia **51**, 5743 (2003), DOI: 10.1016/j.actamat.2003.08.032.

[2] Y.T. Zhu, G. T. Langdon, Materials Science and Engineering A **409**, 234 (2005), DOI: 10.1016/j.msea.2005.05.111.

[3] K. Konopka, L. Litynska-Dobrzynska, J. Dutkiewicz, Archives of Metallurgy and Materials **58**, 501, (2013), DOI: 10.2478/amm-2013-0026.

[4] S. Rusz et al., Archives of Metallurgy and Materials **59**, 359, (2014), DOI: 10.2478/amm-2014-0060.

[5] M. Gajewska, J. Dutkiewicz, J. Morgiel, Journal of Alloys and Compounds **586**, 423, (2014), DOI: 10.1016/j.jallcom.2012.10.055.

[6] A. Kováčová et al., Acta Metallurgica Slovaca **16**, 91 (2010).

[7] M.J. Mayo, Nanostructured Materials **9**, 717 (1997).

[8] M.J. Mayo, J.R. Seidensticker, Dynamic grain growth as the key to superplasticity?, Proceedings of the TMS Fall Meeting, 1999 Julia R. Weertman Symposium; Cincinnati, OH, 179-190 (1999).

[9] H.E. Schaefer et al., Nanostructured Materials **6**, 869 (1995).

[10] Yu.R. Kolobov, G.P. Grabovetskaya, I.V. Ratochka, K.V. Ivanov, Nanostructured Materials **12**, 1127 (1999), DOI: 10.1016/S0965-9773(99)00311-6.

[11] Yu.R. Kolobov, G.P. Grabovetskaya, K.V. Ivanov, M.B. Ivanov, Interface Science **10**, 31 (2002), DOI: 10.1023/A:1015128928158.

[12] C.C. Koch, Nanostructured Materials **9**, 13 (1997).

[13] X. Zhang, H. Wang, R.O. Scattergood, J. Narayan, C.C. Koch, Materials Science and Engineering A **344**, 175 (2003), DOI: 10.1016/S0921-5093(02)00422-7.

[14] R. Bidulsky, J. Bidulska, M. Actis Grande, High Temperature Materials and Processes **28**, 337 (2009).

[15] T. Kvackaj et al., Micron **43**, 720 (2012), DOI: 10.1016/j.micron.2012.01.003.

[16] H. Gleiter, Progress in Materials Science **33**, 223 (1989).

[17] P.G. Sanders, G.E. Fougere, L.J. Thompson, J.A. Eastman, J.R. Weertman, Nanostructured Materials **8**, 243 (1997).

[18] U. Erb, Nanostructured Materials **6**, 533 (1995).

[19] A.M. El-Sharik, U. Erb, G. Palumbo, K.T. Aust, Scripta Metallurgica et Materiala **27**, 1185 (1992).

[20] R.Z. Valiev, T.G. Langdon, Progress in Materials Science **51**, 881 (2006), doi: 10.1016/j.pmatsci.2006.02.003.

[21] M. Besterci, T. Kvačkaj, L. Kováč, K. Sulleiová, Kovove Materialy **44**, 101 (2006).

[22] M. Janeček, B. Hadzima, R.J. Hellmig, Y. Estrin, Kovove Materialy **43**, 258 (2005).

[23] B. Hadzima et al., Materials Science Forum **503-504**, 883 (2006).

[24] N. Izairi, F. Ajredini, M. Ristova, A. Vevecka-Priftaj, Acta Metallurgica Slovaca **19**, 302 (2013), DOI: 10.12776/ams.v19i4.170.

[25] L. Navrátilová, L. Kunz, F. Nový, R. Mintách, Acta Metallurgica Slovaca **19**, 88 (2013), DOI: 10.12776/ams.v19i2.92.

[26] M. Kulczyk, J. Skiba, W. Pachla, Archives of Metallurgy and Materials **59**, 163, (2014), DOI: 10.2478/amm-2014-0026

[27] B. Leszczynska-Madej, P. Palka, M. Richet, Archives of Metallurgy and Materials **59**, 313, (2014), DOI: 10.2478/amm-2014-0051

[28] R. Kočiško et al., Chemicke Listy **104**, s330 (2010).

[29] M. Nemoto, Z. Horita, M. Furukawa, T.G. Langdon, Metals and Materials International **4**, 1181 (1998).

[30] W. Wei, G. Chen, J.T. Wang, G. L. Chen, Rare Metals **25**, 697 (2006), DOI: 10.1016/S1001-0521(07)60015-1.

[31] Y. Ma, M. Furukawa, Z. Horita, M. Nemoto, R.Z. Valiev, T.G. Langdon, Materials Transactions JIM **37**, 336 (1996).

[32] S.X. McFadden, R.S. Mishra, R.Z. Valiev, A.P. Zhilyaev, A.K. Mukherjee, Nature **398**, 684 (1999), DOI: 10.1038/19486.

[33] Z. Horita, T. Fujinami, M. Nemoto, T.G. Langdon, Metallurgical and Materials Transactions A **31**, 691 (2000).

[34] Y.T Zhu, T.G. Langdon, JOM **56**, 58 (2004).

[35] R.Z. Valiev, I.V. Alexandrov, Y.T. Zhu, T.C. Lowe, Journal of Materials Research **17**, 5 (2002).

[36] T. Kvackaj et al., Materials Letters **64**, 2344 (2010), DOI: 10.1016/j.matlet.2010.07.047.

[37] A. Rusinek, J.R. Klepaczko, International Journal of Plasticity **17**, 87 (2001), DOI: 10.1016/S0749-6419(00)00020-6.

[38] A. Niechajowicz, A. Tobota, Archives of Civil and Mechanical Engineering **8**, 129 (2008).

[39] A. Mishra, et al., Acta Materialia **56**, 2770 (2008), DOI: 10.1016/j.actamat.2008.02.023.

[40] P.J. Blau, Friction and Wear Transitions of Materials, Noyes Publications/Park Ridge, NJ 1989.

[41] T. Hanlon, A.H. Chokshi, M. Manoharan, S. Suresh, International Journal of Fatigue **27**, 1159 (2005), DOI: 10.1016/j.ijfatigue.2005.06.036.

[42] Z. Han, B. Yao, K. Lu, Acta Metallurgica Sinica **50**, 238 (2014), DOI: 10.3724/SP.J.1037.2013.00810.

[43] Z. Han, Y. Zhang, K. Lu, Journal of Materials Science and Technology **24**, 483 (2008).

[44] R. Bidulský, M. Actis Grande, J. Bidulská, T. Kvačkaj, Materiali in Tehnologije **43**, 303 (2009).

[45] J. Kovacik, M. Balog, S. Emmer, Kovove Materialy **52**, 71 (2014), DOI: 10.4149/km2014271.

[46] E.C. Teague, F.E. Scire, T.V. Vorburger, Wear **83**, 61 (1982).

[47] K.J. Stout, E.J. Davis, Wear **95**, 111 (1984).

[48] E.P. Whitenton, P.J. Blau, Wear **124**, 291 (1988).

[49] Y. Wang, L. Tingquan, Wear **194**, 44 (1996).

[50] M. Rosso, G. Scavino, Surface Engineering **14**, 217 (1998).

[51] R. Bidulský, M. Actis Grande, High Temperature Materials and Processes **27**, 249 (2008).

[52] J. Bidulská, R. Bidulský, M. Actis Grande, Acta Metallurgica Slovaca **16**, 146 (2010).

[53] R. Bidulský, J. Bidulská, M. Actis Grande, High Temperature Materials and Processes **32**, 467 (2013).

[54] R. Bidulský, J. Bidulská, F. Arenas, M. Actis Grande, High Temperature Materials and Processes **31**, 13 (2012).

[55] K. Bryla et al., Archives of Metallurgy and Materials **58**, 481 (2013), DOI: 10.2478/amm-2013-0022.

[56] J. Bidulska et al., Archives of Metallurgy and Materials **58**, 371 (2013), DOI: 10.2478/amm-2013-0002.

[57] J. Bidulska et al., Kovove Materialy **46**, 339 (2008).

[58] T. Kvackaj et al., Archives of Metallurgy and Materials **58**, 407 (2013), DOI: 10.2478/amm-2013-0008.

Received: 20 September 2014.